ACS APPLIED MATERIALS & INTERFACES

RESEARCH ARTICLE

www.acsami.org

Gold-Nanoparticle-Functionalized In_2O_3 Nanowires as CO Gas Sensors with a Significant Enhancement in Response

Nandan Singh, Raju Kumar Gupta, and Pooi See Lee*

School of Materials Science and Engineering, Nanyang Technological University, 50 Nanyang Avenue, Singapore 639798

ABSTRACT: We present the room-temperature sensing of gold nanoparticle (AuNP)-functionalized In_2O_3 nanowire field-effect transistor (NW-FET) for low-concentration CO gas. AuNPs were functionalized onto In_2O_3 nanowires via a self-assembled monolayer of *p*-aminophenyltrimethoxysilane (APhS-SAM). The nanowires were mounted onto the Au electrodes with both ends in Schottky contacts. High sensor response toward low concentration of CO gas (200 ppb-5 ppm) at room temperature is achieved. The presence of AuNPs on the surface of In_2O_3 nanowire serves to enhance the CO oxidation due to a higher oxygen ion-chemisorption on the conductive AuNP surfaces. Detailed studies showed that the sensing capabilities were greatly enhanced in comparison to those of bare nanowires or low coverage of Au NP-decorated nanowires. When the sensor is exposed to CO, the CO molecules interact with the preadsorbed oxygen ions on the AuNP surface. The CO oxidation on the AuNPs leads to the transfer of electrons into the semiconducting In_2O_3 nanowires and this is reflected as the change in conductance of the NW-FET sensor. This work provides a promising approach for fabricating nanowire devices with excellent sensing capabilities at room temperature.

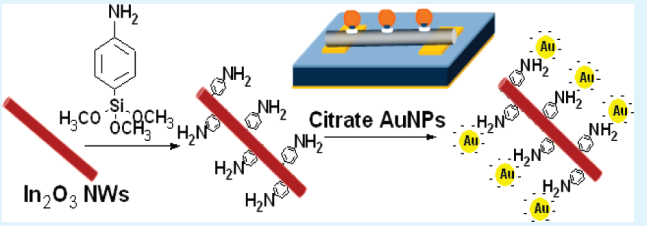

KEYWORDS: In_2O_3 nanowire, Au nanoparticles, field-effect transistor, functionalization, chemisorption, sensor

1. INTRODUCTION

Metal oxide (MOx) semiconducting nanowires are among the most promising materials systems for conductometric gas sensors with the advantages such as large surface-to-volume ratio, higher crystallinity and better stoichiometric control.[1,2] These systems function by converting surface chemical processes, often catalytic processes, into observable conductance variations in the nanowire. Nanocrystalline In_2O_3 sensors are well-known for their applications in the detection of toxic gases such as NO_2, CO, NH_3, etc.[3−5] In_2O_3-based sensors have been found attractive for the selective detection of CO gas.[6] The transduction principle used for the detection of CO is the modification of the surface electrical conduction properties of In_2O_3 by the adsorption and reaction of CO on its surface. The near-surface region becomes depleted of electrons due to the chemisorbed oxygen species.[1] In the presence of a reducing gas (e.g., CO), a chemical reaction between gas molecules and chemisorbed oxygen species leads to electron transfer back into the nanowire, thereby increasing the conductivity.[1] Adsorption and desorption of gas molecules on the surface of metal oxides are both thermally activated processes, which cause the response and recovery times to be usually slow at room temperature. Development of room-temperature gas sensors has very important advantages such as low power consumption, simple system configuration, reduced explosion hazards and longer device lifetime. Single NW-FET based sensors have shown the capability of room temperature operation,[3,4,7,8] allowing gas molecules to directly interact with the single-crystalline nanowire and alter their electronic property, which reflects as a change in the conductance of the device.

The reaction of the surface chemisorbed species with the surrounding gases is critical in the sensing mechanism of the sensor. Because of the lack of selectivity of oxide solid-state sensors to CO, additional noble metals such as Ag, Au, Pd, and Pt as catalytic additives is often needed.[9−12] It is widely accepted that the presence of noble metal elements (Pt, Pd, Au, etc.)[13,14] on the surface of a metal oxide enhances the interaction of reducing gases with the adsorbed oxygen on the surface. These augmented oxide nanowires have attracted great attention in sensors research. Among the various metal catalyst particles, Au is the most widely used and explored catalyst for CO oxidation. Au atoms are known to be reactive for CO oxidation even at 30−40 K.[15] However, the mechanisms for oxygen adsorption on supported Au particle and activation are highly controversial. Several models have been proposed to resolve the controversy on the role of the support material. Valden et al.[16] proposed that oxygen adsorption proceeds directly on the Au particle. One of the widely accepted models proposed that the oxygen adsorption occurs on the support (or at the metal−support interface),[17,18] possibly on oxygen vacancies,[19] which are present on MOx such as TiO_2, Fe_3O_4, In_2O_3, or ZnO. Another model proposed that that oxygen adsorbing on the support dissociates immediately, producing lattice oxygen, which can subsequently react at the interface or after a spillover of oxygen to the gold metal.[20]

Higher metal loading is required in order to achieve higher catalytic oxidation of CO. Different techniques have been used to achieve higher metal loading with uniform particle distribution. Kolmakov et al.[21] performed in situ deposition of Pd nanoparticles in the reaction chamber where the gas sensing measurements were carried out to ensure that the observed behavioral

Received: December 22, 2010
Accepted: June 8, 2011
Published: June 08, 2011

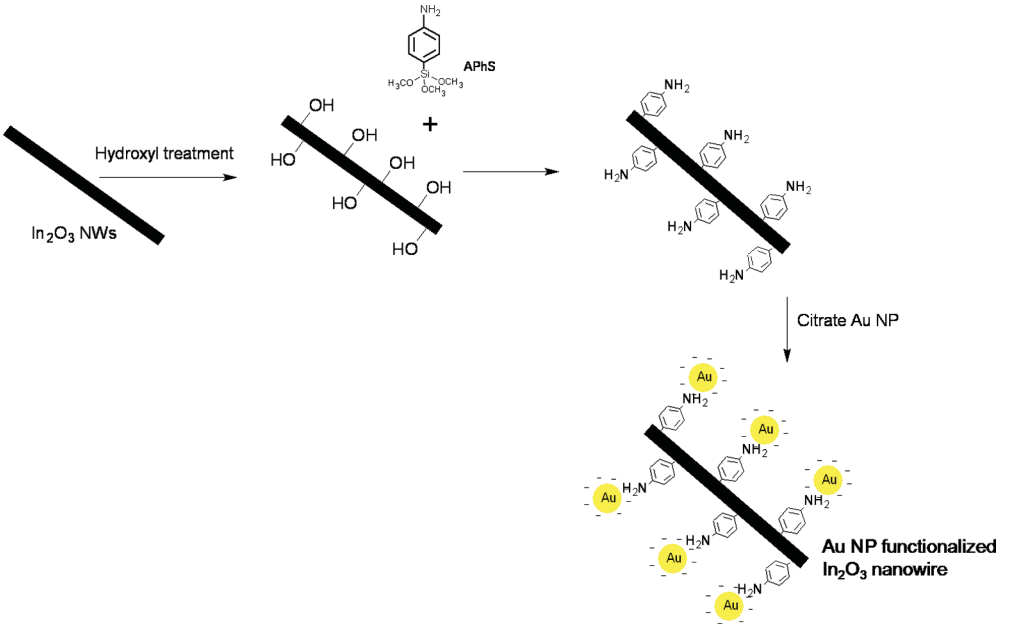

Figure 1. Schematic for citrate-capped AuNP functionalization on In_2O_3 nanowire.

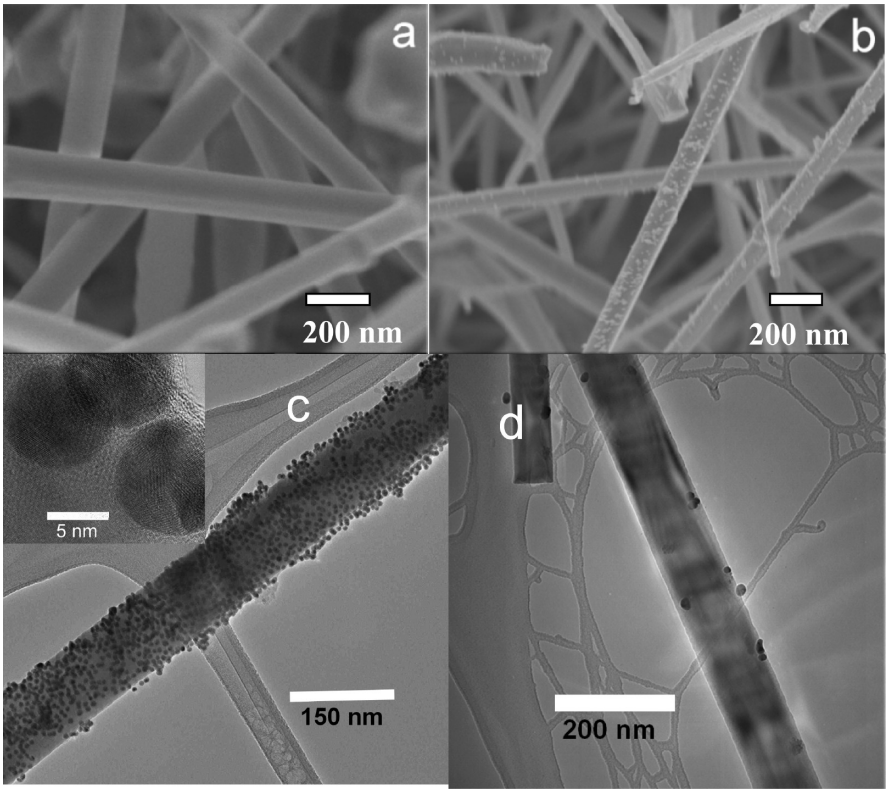

Figure 2. FESEM images of (a) as-synthesized In_2O_3 nanowires and (b) AuNP-functionalized In_2O_3 nanowires. TEM images of (c) AuNP-functionalized In_2O_3 nanowires using SAM layer and (d) AuNP-decorated In_2O_3 nanowires without SAM layer.

alteration was due to the Pd immobilization and the sensor response strongly depends on the surface coverage of metal particles. However, despite the higher coverage attained using in situ deposition of metal particles, the nonselective deposition results in unavoidable deposition on the isolation region adjacent to the channel leading to extraneous conductive paths.[21] This can affect drain current as a result of electron conductance when the metal nanoparticles exceed the percolation threshold. Self-assemblies have been used in recent years to organize nanoparticles onto the surface of the nanowires.[22,23] Zhang et al.[22] have obtained a selective sensor response for low concentration of H_2S gas using ZnO nanowire modified with Pd nanoparticles through

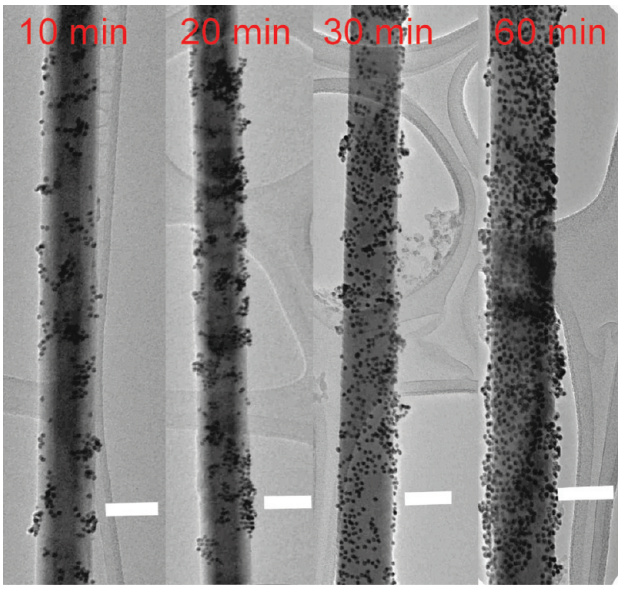

Figure 3. TEM images of the nanowires with different Au loading time during immobilization. The scale bars in all images are 100 nm.

self-assemblies. In this work, we present a selective solution assembly approach to obtain high coverage of AuNPs on the nanowire surface through deposition of presynthesized AuNPs over APhS-SAM functionalized nanowires.

Apart from the nanowire channel, sensor response in a NW-FET device also depends on the contact resistance at two ends of the nanowire. Contact resistance modulation in nanowire sensing has proved to be an effective way to improve gas sensing.[24−26] Recently, we have found that Schottky contact devices show a superior response to the reducing gas (CO),[27] in agreement with other similar findings.[24,25] Herein, we have utilized the approach of functionalization of nanowire channel by AuNPs on Schottky devices to enhance the sensor response toward CO gas sensing at room temperature. We have obtained highly sensitive devices for CO (down to ppb level) gas sensing at room temperature, one of the best reported performance for room-temperature CO sensing.[4,14,27,28]

2. EXPERIMENTAL SECTION

2.1. Materials. *p*-Aminophenyltrimethoxysilane (APhS) was purchased from Gelest, and used as received. Hydrogen tetrachloroaurate (III) trihydrate ($HAuCl_4.3H_2O$) (≥99.9%, Aldrich; *corrosive, handle with care*), sodium citrate (meeting USP testing specifications, Sigma), ethanol (≥99.5%, Merck), toluene (≥99%, Merck), and methanol (≥99.5%, Merck) were used as-received.

2.2. Synthesis of In_2O_3 Nanowires. In_2O_3 NWs were grown in a horizontal CVD furnace at a source temperature of 900 °C under argon flow rate of 50 sccm as earlier reported.[29] The source for the growth was In_2O_3 with graphite powder. During the deposition, argon gas flow rate was fixed at 50 sccm and the pressure inside the quartz tube was maintained at 1 mbar. Si substrates with 9 nm gold layer were kept downstream and the substrate temperature ranges from 400 to 550 °C with deposition duration of 60 min. The morphology and crystal structure of the as grown nanostructures was studied under field emission scanning electron microscopy (FESEM) on a JEOL 7600F scanning electron microscope operated at 5 kV and transmission electron microscopy (TEM) (JEOL JEM-2100F) operated at 200 kV.

2.3. Synthesis of Citrate-Stabilized Gold Nanoparticles. Gold nanoparticles were prepared according to the method reported previously.[30] Specifically, 0.012 g of $HAuCl_4.3H_2O$ was dissolved in 30 mL of deionized (DI) water giving a 1 mM solution, which was then refluxed at ca. 115 °C for 10 min. Six milliliters of 38.8 mM sodium citrate also dissolved in DI water was added to the refluxing solution. The color of the mixture evolved gradually from gray to purple and finally to wine red. Refluxing was continued for another 10 min and then was stopped to let the resulting solution cool to room temperature.

2.4. Immobilization of AuNPs on In_2O_3 Nanowires. *2.4.1. Substrate Preparation.* In_2O_3 nanowires deposited on Si substrate was treated with 1:1:5 (v/v) mixture of 30% hydrogen peroxide, 30% (aq) NH_4OH and DI water at 75 °C for 45 min. Substrate was then copiously rinsed with deionized water, blown dry with nitrogen, and dried at 100 °C under a vacuum for 30 min. This cleaning procedure creates a surface rich in hydroxyl groups at the In_2O_3 nanowires surface to facilitate the subsequent silanization process.[31,32]

2.4.2. Self-Assembly of Aminosilane. Assembly of aminosilane was performed as described elsewhere,[33] wherein the hydroxyl terminated substrates were rinsed with toluene and then immersed in a 3 mM APhS solution in toluene for 2 h. Subsequently, the substrate was removed from the solution, rinsed with toluene and then with acetone, and finally blown dry with nitrogen.

2.4.3. Immobilization of Gold Nanoparticles. The silane treated Si substrate was immersed in the freshly prepared AuNPs solution for 60 min, rinsed thoroughly with DI water, and then baked at 110 °C for 5 min to remove residual moisture. Details of various deposition steps are shown in Figure 1.

2.5. Sensor Device Fabrication. In_2O_3 nanowire-based devices were fabricated on a highly doped n-type silicon wafer with a 100 nm SiN_x high-k dielectric layer. Standard optical-lithography followed by Cr/Au (10/50 nm) deposition and liftoff was used to define the contact electrodes. The highly conductive heavily doped Si substrate (resistivity 0.005 Ω cm) was used as a global back gate. The In_2O_3 nanowires were removed from the silicon substrates by sonication in Isopropyl alcohol (IPA) solution. IPA solution containing In_2O_3 nanowires and AuNPs functionalized In_2O_3 nanowires were drop-casted onto the patterned Si substrate. After drying, locations of nanowires on the pads (electrodes) were identified for fabricating nanowire-based field-effect transistor (FET) structures. Electrical and sensing measurements on the nanowire FET were done in a Keithley 4200-SCS semiconductor characterization system, attached with an optical microscope and sensing gases with gas controller. I_d-V_d transistor characteristics on a single NW-FET were performed under different applied V_g ranges from 5 V to −15 V with a voltage step of −5 V. In I_d-V_g transistor characteristics I_d was measured for a range of V_g (−10 to 5 V) under a constant applied V_d bias of 2 V. The responses of the NW-FET device to CO gas were evaluated by measuring the resistance/conductance change upon exposure to various concentrations of CO gas in a dynamic gas flow chamber under a constant gas flow rate of 300 sccm. Various concentrations of CO gas were obtained by diluting a premixed concentration of CO gas in N_2. The sensor response (S) toward CO gas was calculated as the ratio of the resistances of the device in air (R_a) to that in the CO gas (R_g) at room temperature and a relative humidity (RH) of 50%.

3. RESULTS AND DISCUSSION

APhS-SAM layer was used to functionalize the AuNPs on the nanowire surface. As shown in the FESEM image (Figure 2a), the as-grown nanowires have a diameter of 150−200 nm and Figure 2b shows FESEM image after functionalization of the citrate stabilized AuNPs on APhS-SAM-treated In_2O_3 nanowires. AuNPs were functionalized on amine-terminated surface because of amine−gold interaction. The nanowires show a high

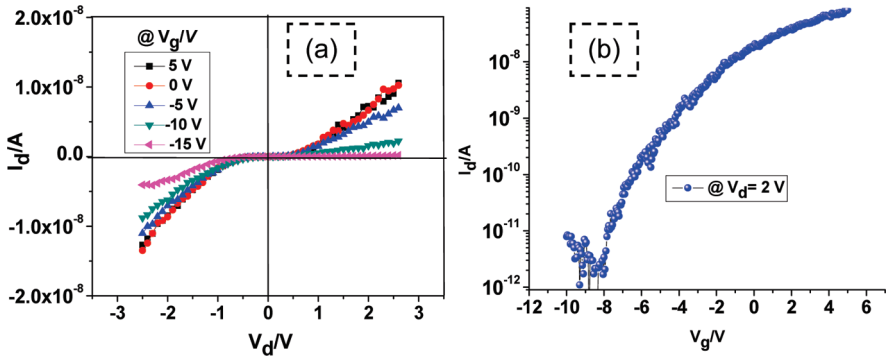

Figure 4. Transfer characteristics of a single nanowire FET, (a) I_d-V_d curves showing Schottky type of device characteristics, (b) I_d-V_g characteristics at a drain voltage of 2 V.

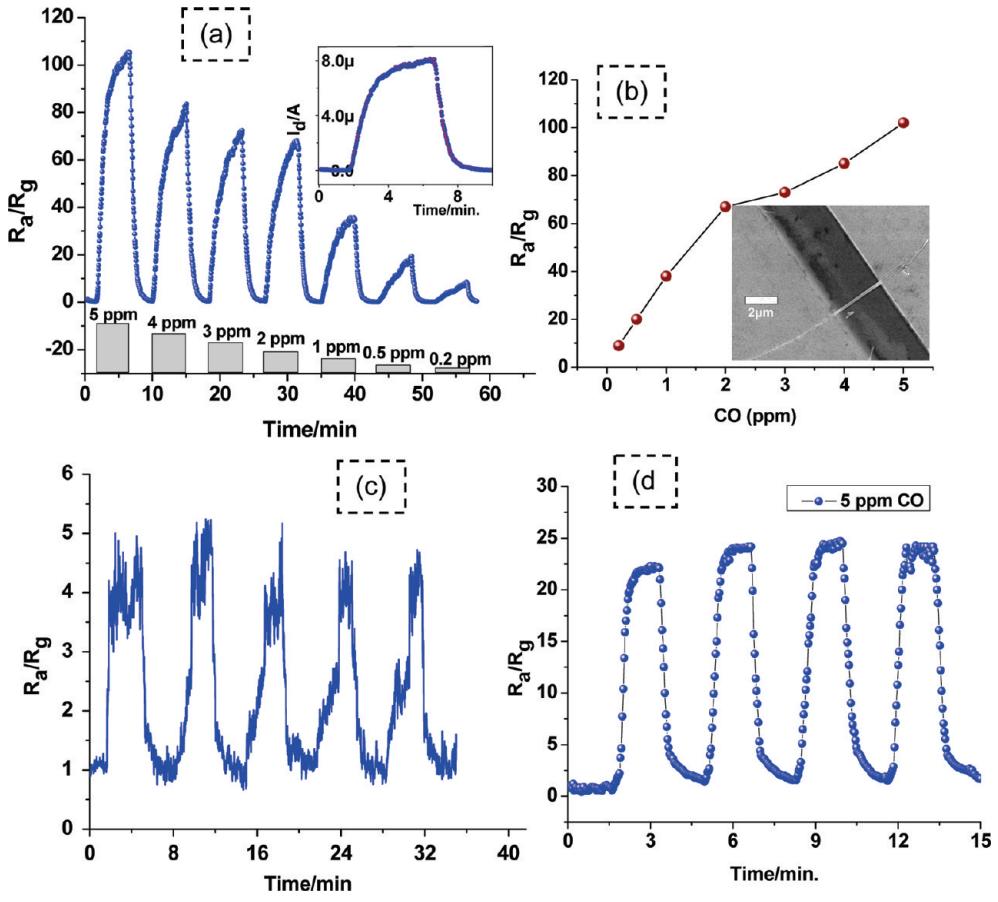

Figure 5. Gas testing plots for sensor operated at room temperature; (a) response plot for the AuNPs F-NW-FET (standard 60 min loading time), when exposed to 5−0.2 ppm CO and inset shows a zoomed view of the I_d-time plot for 5 ppm CO gas, (b) sensor response plot for CO gas at room temperature for the same device as shown in the inset. The drain and gate voltages were kept constant at V_d = 2 V and V_g = −5 V, respectively, during sensing experiment; (c) sensor response toward 5 ppm CO gas in different cycles using a AuNPs D-NW-FET device, and (d) the sensor response toward 5 ppm CO gas from the AuNPs F-NW-FET device for 10 min Au loading time.

coverage of AuNPs with sizes of around 10 nm as shown in the TEM image (inset of Figure 2c). To evaluate the effect of AuNPs coverage on nanowire surface, we have fabricated two types of devices: in the first type of devices, an APhS-SAM layer was used to functionalize AuNPs on nanowire surface with higher surface coverage (Figure 2c) and the devices were termed as AuNPs functionalized In_2O_3 NW-FET (AuNPs F-NW-FET). The second type of devices were fabricated without using SAM layer where AuNPs solution was directly added to the In_2O_3 nanowire solution and a low surface coverage of AuNPs was observed (Figure 2d) because of physical adsorption, these devices were termed as AuNPs decorated In_2O_3 NW-FET (AuNPs D-NW-FET). Figure 3 Shows the TEM images for different Au loading time using APhS-SAM layer.

Figure 4(a) shows the I_d-V_d characteristics at different gate voltage (V_g) for the AuNPs F-NW-FET. Nonlinear and

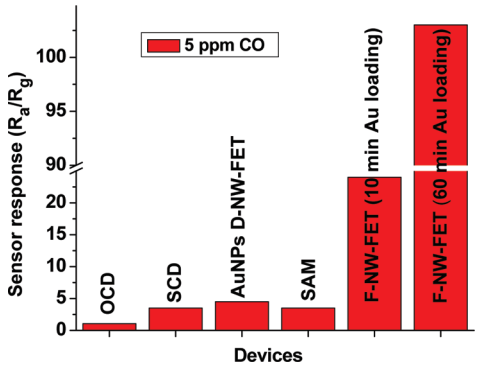

Figure 6. Sensor response comparison for 5 ppm CO gas obtained from; OCD (Ohmic contacted device), SCD (Schottky contacted device), AuNPs D-NW-FET, nanowire-coated with only APhS SAM, AuNPs F-NW-FET for 10 and 60 min Au loading, respectively.

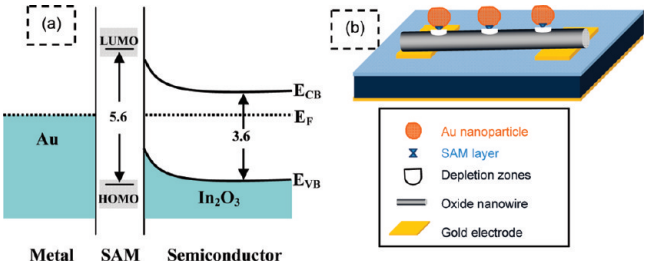

Figure 7. Illustration of (a) band diagram of the metal-SAM-semiconductor system, (b) schematic of the AuNPs F-NW-FET device, showing the formation of depletion regions (white color) underneath the AuNPs.

asymmetrical characteristics indicate Schottky nature of the metal-semiconductor (MS) junction with large resistance of 290 MΩ at V_g = −5 V. A threshold voltage of −8.5 V with a large sub threshold swing (∼1 V/decade) at a fixed V_d of 2 V was obtained from the I_d−V_g plot for the same device, shown in Figure 4b. Similar Schottky behavior was obtained for devices of AuNPs D-NW-FET and samples without AuNPs. A larger threshold voltage of −13.6 V with a smaller threshold voltage swing of ∼185 mV/decade was previously found for Ohmic contacts using the same nanowires.[27]

To understand the effect of AuNPs coverage on nanowire surface, we tested both devices for the detection of pollutant gas carbon monoxide (CO) at room temperature. Drain voltage (V_d) was kept constant at 2 V and gate voltage (V_g) was kept at −5 V (within the threshold region of the F-NW-FET) during all the measurements. The sensing response of the bare single In_2O_3 Schottky device (without using AuNPs) is reported elsewhere,[27] where it has been observed that Schottky type devices exhibit better sensing responses toward CO gas in comparison to their Ohmic counterpart due to Schottky barrier height (SBH) modulation during CO gas exposure. Sensor response of the AuNPs F-NW-FET for 0.2−5 ppm CO gas is shown in Figure 5a. A sensor response (S) of nearly 104 was obtained using AuNPs F-NW-FET toward 5 ppm CO gas with a response time of ∼130 s and recovery time of ∼50 s (Figure 5a). We were able to detect distinct electrical changes for the CO gas concentration down to 0.2 ppm using AuNPs F-NW-FET at room temperature. Figure 5(b) shows the sensitivity plot for the CO gas at room temperature under 50% RH. A decreasing slope with increasing concentration of CO gas indicates saturation in response toward higher gas concentration (Figure 5b). A lower sensor response of ∼4.5 with a shorter response and recovery times of 17 and 12 s respectively, was obtained for 5 ppm CO gas exposure (Figure 5c) using AuNPs D-NW-FET. The significant improvement in sensor response for AuNPs F-NW-FET is almost 23 times (Figure 5a) higher than the AuNPs D-NW-FET and almost 30 times better than bare nanowire sensor (S = 3.5, for 5 ppm CO using SCD).[27] The larger time constants (response and recovery time) for AuNPs F-NW-FET are attributed to the slow electronic transport through APhS-SAM layer. To confirm the role of AuNPs coverage in AuNPs F-NW-FET devices we have used nanowires with different Au loading time (e.g., 10, 20, 30 and 60 min) as shown in Figure 3. Nanowires showed a lower AuNPs coverage for 10 and 20 min. The device with 10 min Au loading was tested for 5 ppm CO gas under similar operating conditions and a sensor response of ∼23.5 was obtained as shown in Figure 5d. The lower sensor response (in comparison of ∼104 of 60 min Au loading device) evidently shows the importance of high loading of metal nanoparticles. The comparison of sensor responses from different devices is shown in Figure 6. It is noteworthy that the nanowires coated with only APhS SAM did not improve the sensor response, corroborating our findings on the role of metal nanoparticles.

It is well-known that oxygen chemisorption on the surface of MOx nanowires plays an important role in the CO oxidation and hence electrical transport properties.[1,6] The chemisorption of oxygen species depends strongly on temperature and the surface characteristics of the nanowire material.[34,35] A room-temperature thin film sensor shows weak sensor response mainly due to the existence of large number of grain boundaries in the polycrystalline film, which provides large energy barriers on the electrons percolation path. This necessitates the need of thermal activation to improve gas adsorption/desorption. In contrast, sensor response at room temperature can be found in single-nanowire sensors mainly due to the single-crystalline nature providing better conductivity and reduced energy barriers for the current injection across the device with the assistance of gate control. In the nanowire transistor configuration, the electric field applied at the gate electrode modulates the carrier concentration, which in turn significantly affects adsorption and desorption behaviors of gas molecules or gas sensitivity.[36]

The presence of metal nanoparticles with high work function on the surface of n-type semiconducting nanowire leads to nanoscopic depletion region (nano-Schottky barriers, due to difference in work function) at MS interface, which modulates the device conductance.[21,37,38] The depletion region around nanoparticle improves the sensor response due to the modulation of the nano-Schottky barriers (and hence width of the conduction channel) (Figure 7). In addition, a well-known "spillover effect" has to be taken into account; that the metal nanoparticles catalytically activate the dissociation of molecular species, whose atomic products then diffuse to the metal oxide support.[21,37−40] The size of the spillover zone depends on the particle size and experimental conditions.[41] At higher particle coverage, the spillover zones essentially cover most of the nanowire surface in F-NW-FET, which increase the CO oxidation into CO_2 because of the availability of increased chemisorbed gas ions. We have observed that sensor response depends dramatically on the degree of metal nanoparticle coverage of the nanowire surface which corroborates with the previous results.[21] High coverage of the AuNPs on the nanowire surface has been tailored with the use

of APhS-SAM layer in this work. The sensing mechanism of such devices can be explained in the following steps: first is the effect of higher AuNPs coverage on nanowire; second, the role of SAM layer on sensing enhancement and electronic transport through it; and finally, SBH modulation in a Schottky device during gas exposure.

Immobilization of AuNPs facilitates adsorption of gaseous species on the nanoparticle surfaces at room temperature because of the higher surface defects available in nanoparticles surface, highly conductive nature, and availability of free electrons in gold.[11,14,42,43] In this work, by using the fact that gold is a good catalyst for the CO oxidation,[42,43] the high density of AuNPs attached to the nanowire increases the CO oxidation into CO_2, which reflects as an increased conductance of the nanowire-channel. In the present Au−In_2O_3 nanowires system the conductance changes when the CO gas is introduced into the test chamber due to the exchange of electrons between ionosorbed species and Au decorated In_2O_3 nanowires. Higher surface coverage by AuNPs increases the CO oxidation in to CO_2 via catalytic activation. On the other hand a smaller sensor response of 4.5 (for AuNPs D-NW-FET) was obtained compare to the sensor response of 3.5 for bare NW-FET in ref.[27] The small enhancement in sensor response of AuNPs D-NW-FET devices can be attributed to the low AuNPs coverage as shown in the TEM images (Figure 2d). It is well-documented that gold particle sizes influence the CO oxidation. The increasing oxidation with smaller particle size was explained by an enhanced dissociative adsorption of oxygen on small gold particles, due to a higher density of reactive defect sites (edge, kink, or step sites)[44] or a gradual change in the electronic structure at decreasing size.[16] However it has been observed that the particle size dependence CO oxidation is much influenced by the support material.[17,45−47] For inert support materials (e.g., Au/SiO_2, Au/Al_2O_3), the critical particle diameter is reported around 2 nm.[17,45] For active support materials (e.g., Au/Fe_2O_3, Au/TiO_2), the gold particle size plays a secondary role.[17,46] Even catalysts with gold particles as large as 12 nm (Au/Fe_2O_3) or 30 nm (Au/TiO_2) still exhibit catalytic effect comparable to those with small Au particle sizes.[17]

The primary role of the APhS-SAM layer is to increase the density of the AuNPs on the nanowire surface which can be clearly seen in TEM image (Figure 2c). The presence of the SAM layer can affect the volume of the depletion region underneath nanoparticle, as transportation of electrons between nanowire and nanoparticle through APhS-SAM molecule would not be as fast as that without APhS-SAM. Studies have shown that the electronic transport through SAM layers could be in the form of tunneling, thermionic or hoping.[48] The conduction mechanism is expected to be tunneling when the Fermi levels of contacts lie within the large HOMO−LUMO gap for short length molecules, as for the case of alkane thiolmolecular system (∼4.5 eV).[49] We have estimated a HOMO−LUMO gap of ∼5.633 eV for the APhS-SAM (thickness ∼1 nm) using Gaussian simulation. Furthermore, it is well documented that polar SAMs (e.g., APhS-SAM) can tune the electronic properties of their interfaces with semiconductors/metals by shifting the surface potential/dipole,[50,51] carrier density,[52,53] electron affinity[54,55] and work function [56,57]. A polar monolayer introduces a net electrical dipole perpendicular to the surface/interface.[51,58] This results in a potential shift that modifies the work function and electron affinity at a surface and changes the band offset and band bending at an interface. Thus, the Au/SAM interface behaves as an active support system where the size of Au particles plays secondary role. Due to the slower electronic transport through APhS-SAM layer, F-NW-FET shows a larger response and recovery time (130 and 50 s, respectively) in comparison to D-NW-FET (17 and 12 s for 5 ppm CO gas).

In a single NW-FET, the presence of potential barrier at the MS interface plays a crucial role in the charge transportation across the interface.[24−26] The increased conductance (as seen in Figure 5a inset) of the channel has another advantage; due to the large change in the relative conductance of the nanowire channel, lowering of SBH takes place at the MS interface and a large change in the relative current (100 nA to ∼8 μA for 5 ppm CO gas in 300 s shown in the inset of Figure 5a) was observed when the device was operated under forward bias of 2 V. In such devices, potential barriers are present at the two ends of the nanowire and these are connected in series with the nanowire channel resistance; as a result the device shows a large resistance initially. By using the AuNPs functionalization to the nanowire channel, all three resistances in series are decreased because of the transfer of electrons from the CO molecules to the nanowire channel, which results in lowering of the net resistance of the device. As a result of the drastic decrease in net resistance of the device, a large relative change in the device conductivity was resulted. The significant enhance in the sensor response at room temperature is mainly attributed to the higher AuNPs density at the nanowire surface. The Schottky barrier in this study has been controlled mainly by the contact material properties.

4. CONCLUSIONS

In summary, a highly sensitive device for the CO gas sensing at room temperature has been demonstrated by combining the Schottky contact effect with a metal nanoparticle functionalized nanowire channel. APhS-SAM modification of In_2O_3 nanowires with amine terminated groups resulted in a high coverage of AuNPs attached on the nanowire surface. In addition to the high density of AuNPs on the NW surface, the utilization of the Schottky contact at the nanowire-electrode junction plays a crucial role in the sensor response. The modulation of SBH due to the higher number of electrons transferred to the nanowire channel during CO oxidation made the device highly sensitive toward CO gas, which is found to be dependent on the degree of coverage of the AuNPs on the In_2O_3 nanowire surface. The comparative sensing performances of single nanowires before and after surface decoration with Au catalyst nanoparticles show significant improvement in sensitivity toward reducing gas like CO.

AUTHOR INFORMATION

Corresponding Author
*E-mail: pslee@ntu.edu.sg.

ACKNOWLEDGMENT

N.S. acknowledges scholarship awarded by NTU. The authors thank Dr. G. Liu for providing support on the simulation, W. Ye for providing technical support, and Dr. E. Comini for the insightful discussion.

REFERENCES

(1) Comini, E.; Faglia, G.; Sberveglieri, G.; Pan, Z. W.; Wang, Z. L. *Appl. Phys. Lett.* **2002**, *81*, 1869–1871.
(2) Kolmakov, A.; Zhang, Y.; Cheng, G.; Moskovits, M. *Adv. Mater.* **2003**, *15*, 997–1000.

(3) Zhang, D.; Liu, Z.; Li, C.; Tang, T.; Liu, X.; Han, S.; Lei, B.; Zhou, C. *Nano Lett.* **2004**, *4*, 1919–1924.
(4) Singh, N.; Yan, C.; Lee, P. S. *Sens. Actuators, B* **2010**, *150*, 19–24.
(5) Zhang, D.; Li, C.; Liu, X.; Han, S.; Tang, T.; Zhou, C. *Appl. Phys. Lett.* **2003**, *83*, 1845–1847.
(6) Yamaura, H.; Jinkawa, T.; Tamaki, J.; Moriya, K.; Miura, N.; Yamazoe, N. *Sens. Actuators B.* **1996**, *35*, 325–332.
(7) Zeng, Z. M.; Wang, K.; Zhang, Z. X.; Chen, J. J.; Zhou, W. L. *Nanotechnology.* **2009**, *20*, 045503/1–4.
(8) Kaur, M.; Jain, N.; Sharma, K.; Bhattacharya, S.; Roy, M.; Tyagi, A. K.; Gupta, S. K.; Yakhmi, J. V. *Sens. Actuators, B* **2008**, *133*, 456–461.
(9) Yamazoe, N.; Kurokawa, Y.; Seiyama, T. *Sens. Actuators, B* **1983**, *4*, 283–289.
(10) Voogt, E. H.; Coulier, L.; Gijzeman, O. L. J.; Geus, J. W. *J. Catal.* **1997**, *169*, 359–364.
(11) Haruta, M. *J. New Mater. Electrochem. Syst.* **2004**, *7*, 163–172.
(12) Lim, D. C.; Salido, I. L.; Kim, Y. D. *Surf. Sci.* **2005**, *598*, 96–103.
(13) Vander Wal, R. L.; Hunter, G. W.; Xu, J. C.; Kulis, M. J.; Berger, G. M.; Ticich, T. M. *Sens. Actuators, B* **2009**, *138*, 113–119.
(14) Joshi, R. K.; Hu, Q.; Alvi, F.; Joshi, N.; Kumar, A. *J. Phys. Chem. C* **2009**, *113*, 16199–16202.
(15) Huber, H.; McIntosh, D.; Ozin, G. *Inorg. Chem.* **1977**, *16*, 975–979.
(16) Valden, M.; Pak, S.; Lai, X.; Goodman, D. *Catal. Lett.* **1998**, *56*, 7–10.
(17) Schubert, M.; Hackenberg, S.; Veen, A.; Muhler, M.; Plzak, V.; Behm, R. *J. Catal.* **2001**, *197*, 113–122.
(18) Grunwaldt, J. D.; Baiker, A. *J. Phys. Chem. B* **1999**, *103*, 1002–1012.
(19) Liu, H.; Kozlov, A. I.; Kozlov, A. P.; Shido, T.; Asakura, K.; Iwasawa, Y. *J. Catal.* **1999**, *185*, 252–264.
(20) Tripathi, A. K.; Kamble, V. S.; Gupta, N. M. *J. Catal.* **1999**, *187*, 332–342.
(21) Kolmakov, A.; O.Klenov, D.; Lilach, Y.; Stemmer, S.; Moskovits, M. *Nano Lett.* **2005**, *5*, 667–673.
(22) Zhang, Y.; Xiang, Q.; Xu, J.; Xu, P.; Pan, Q.; Li, F. *J. Mater. Chem.* **2009**, *19*, 4701–4706.
(23) Ramlan, D. G.; May, S. J.; Zheng, J.-G.; Allen, J. E.; Wessels, B. W.; Lauhon, L. J. *Nano Lett.* **2006**, *6*, 50–54.
(24) Wei, T.-Y.; Yeh, P.-H.; Lu, S.-Y.; Wang, Z. L. *J. Am. Chem. Soc.* **2009**, *131*, 17690–17695.
(25) Das, S. N.; Kar, J. P.; Choi, J.-H.; Lee, T. I.; Moon, K.-J.; Myoung, J.-M. *J. Phys. Chem. C* **2010**, *114*, 1689–1693.
(26) Hung, P.; Li, Z.; Wang, Z. L. *Adv. Mater.* **2009**, *21*, 4975–4978.
(27) Singh, N.; Yan, C.; Lee, P. S.; Comini, E. *Nanoscale* **2011**, *3*, 1760–1765.
(28) Marikutsa, A. V.; Rumyantseva, M. N.; Yashina, L. V.; Gaskov, A. M. *J. Solid State Chem.* **2010**, *183*, 2389–2399.
(29) Singh, N.; Zhang, T.; Lee, P. S. *Nanotechnol.* **2009**, *20*, 195605/1–7.
(30) Grabar, K. C.; Freeman, R. G.; Hommer, M. B.; Natan, M. J. *Anal. Chem.* **1995**, *67*, 735–743.
(31) Madeley, J. M.; Richmond, C. R. *Z. Anorg. Allg. Chem.* **1972**, *389*, 92–96.
(32) Zhuravlev, L. T. *Langmuir* **1987**, *3*, 316–318.
(33) Zhang, F.; Srinivasan, M. P. *Langmuir* **2004**, *20*, 2309–2314.
(34) Kohl, D. *Sens. Actuators, B* **1990**, *1*, 158–165.
(35) Franke, M. E.; Koplin, T. J.; Simon, U. *Small* **2006**, *2*, 36–50.
(36) Fan, Z.; Lu, J. G. *Appl. Phys. Lett.* **2005**, *86*, 123510–123512.
(37) Zhdanov, V. P. *Surf. Sci.* **2002**, *512*, 331–334.
(38) Dobrokhotov, V.; McIlroy, D. N.; Norton, M. G.; Abuzir, A.; Yeh, W. J.; Stevenson, I.; Pouy, R.; Bochenek, J.; Cartwright, M.; Wang, L.; Dawson, J.; Beaux, M.; Berven, C. *J. Appl. Phys.* **2006**, *99*, 104302/1–7.
(39) Belmonte, J. C.; Manzano, J.; Arbiol, J.; Cirera, A.; Puigcorbe, J.; Vila, A.; Sabate, N.; Gracia, I.; Cane, C.; Morante, J. R. *Sens. Actuators, B* **2006**, *114*, 881–892.
(40) Dieguez, A.; Vila, A.; Cabot, A.; Romano-Rodriguez, A.; Morante, J. R.; Kappler, J.; Barsan, N.; Weimar, U.; Goepel, W. *Sens. Actuators, B* **2000**, *68*, 94–99.
(41) Bennett, R. A.; Stone, P.; Bowker, M. *Faraday Discuss.* **1999**, *114*, 267–278.
(42) Liu, Z.-P.; Hu, P.; Alavi, A. *J. Am. Chem. Soc.* **2002**, *124*, 14770–14779.
(43) Boronat, M.; Corma, A. *Dalton Trans.* **2010**, *39*, 8538–8546.
(44) Mavrikakis, M.; Stoltze, P.; Norskov, J. K. *Catal. Lett.* **2000**, *64*, 101–106.
(45) Okumura, M.; Nakamura, S.; Tsubota, S.; Nakamura, T.; Azuma, M.; Haruta, M. *Catal. Lett.* **1998**, *51*, 53–58.
(46) Grunwaldt, J. D.; Kiener, C. W.; Wogerbauer, C.; Baiker, A. *J. Catal.* **1999**, *181*, 223–232.
(47) Ma, Z.; Dai, S. *Nano Res.* **2011**, *4*, 3–32.
(48) Wang, W.; Lee, T.; Reed, M. A. *Rep. Prog. Phys.* **2005**, *68*, 523–544.
(49) Boulas, C.; Davidovits, J. V.; Rondelez, F.; Vuillaume, D. *Phys. Rev. Lett.* **1996**, *76*, 4797–800.
(50) Miramond, C.; Vuillaume, D. *J. Appl. Phys.* **2004**, *96*, 1529–1536.
(51) Haick, H.; Ambrico, M.; Ligonzo, T.; Tung, R. T.; Cahen, D. *J. Am. Chem. Soc.* **2006**, *128*, 6854–6869.
(52) Kobayashi, S.; Nishikawa, T.; Takenobu, T.; Mori, S.; Shimoda, T.; Mitani, T.; Shimotani, H.; Yoshimoto, N.; Ogawa, S.; Iwasa., A. *Nat. Mater.* **2004**, *3*, 317–322.
(53) Heimel, G.; Romaner, L.; Zojer, E.; Bredas, J. L. *Nano Lett.* **2007**, *7*, 932–940.
(54) Peor, N.; Sfez, R.; Yitzchaik, S. *J. Am. Chem. Soc.* **2008**, *130*, 4158–4165.
(55) Cohen, R.; KronikS, L.; hanzer, A.; Cahen, D.; Liu, A.; Rosenwaks, Y.; Lorenz, J. K.; Ellis, A. B. *J. Am. Chem. Soc.* **1999**, *121*, 10545–10553.
(56) Boer, B. D.; Handipour, A.; Mandoc, M. M.; Woundenbergh, T. V.; Blom, P. W. M. *Ad. Mater.* **2005**, *17*, 621–625.
(57) Katz, H. E.; Johnson, J.; Lovinger, A. J.; Li, W. *J. Am. Chem. Soc.* **2000**, *122*, 7787–7792.
(58) Natan, A.; Kronik, L.; Haick, H.; Tung, R. T. *Adv. Mater.* **2007**, *19*, 4103–4117.